HHS Public Access

Author manuscript

Magn Reson Med. Author manuscript; available in PMC 2019 December 01.

Published in final edited form as:

Magn Reson Med. 2018 December ; 80(6): 2609–2617. doi:10.1002/mrm.27365.

Chemical exchange rotation transfer (CERT) on human brain at 3 T

Eugene C. Lin[1,2], **Hua Li**[1,2], **Zhongliang Zu**[1,2], **Elizabeth A. Louie**[1,2], **Chris L. Lankford**[1,2], **Richard D. Dortch**[1,2,3], **Mark D. Does**[1,2,3], **John C. Gore**[1,2,3,4,5], and **Daniel F. Gochberg**[1,2,4]

[1]Vanderbilt University Institute of Imaging Science, Nashville, TN

[2]Department of Radiology and Radiological Sciences, Vanderbilt University, Nashville, TN

[3]Department of Biomedical Engineering, Vanderbilt University, Nashville, TN

[4]Deparment of Physics and Astronomy, Vanderbilt University, Nashville, TN

[5]Molecular Physiology and Biophysics, Vanderbilt University, Nashville, Tennessee, USA

Abstract

Purpose—To test the ability of a novel pulse sequence applied *in vivo* at 3T to separate the contributions to the water signal from amide proton transfer (APT) and relayed nuclear Overhauser enhancement (rNOE) from background direct water saturation and semi-solid Magnetization transfer (MT). The lack of such signal source isolation has confounded conventional chemical exchange saturation transfer (CEST) imaging.

Methods—We quantified APT and rNOE signals using a chemical exchange rotation transfer (CERT) metric, MTR_{double}. A range of duty cycles and average irradiation powers were applied, and results were compared with conventional CEST analyses using asymmetry (MTR_{asym}) and extrapolated magnetization transfer (EMR).

Results—Our results indicate that MTR_{double} is more specific than MTR_{asym} and, since it requires as few as three data points, is more rapid than methods requiring a complete Z-spectrum, such as EMR. In white matter, APT (1.5 ± 0.5%) and rNOE (2.1 ± 0.7%) were quantified by using MTR_{double} with a 30% duty cycle and a 0.5 μT average power. In addition, our results suggest MTR_{double} is insensitive to B_0 inhomogeneity, further magnifying its speed advantage over CEST metrics that require a separate B_0 measurement. However, MTR_{double} still has non-trivial sensitivity to B_1 inhomogeneities.

Conclusion—We demonstrated MTR_{double} is an alternative metric to evaluate APT and rNOE, which is fast, robust to B_0 inhomogeneity, and easy to process.

Keywords

CEST; CERT; APT; rNOE; chemical exchange

Correspondence to: Daniel F. Gochberg, Ph.D., Vanderbilt University Institute of Imaging Science, 1161 21st Ave. S, Medical Center North, AAA-3112, Nashville, TN 37232-2310, daniel.gochberg@vanderbilt.edu, Phone: 615-322-8356, Fax: 615-322-0734.

Introduction

Chemical exchange saturation transfer (CEST) imaging can detect solute molecules and their physiological environment (e.g. pH and temperature) through changes in the measured water signal due to the accumulative effects chemical exchange or dipolar coupling (1). In CEST imaging, the water signal as a function of RF irradiation frequency offset is usually obtained. This Z-spectrum contains contributions from broad semi-solid macromolecules (MT), solute chemical exchange sites (such as amine, hydroxyl, and amide protons), and partially restricted carbon bound sites (nuclear Overhauser enhancement, (NOE)). Among these CEST effects, amide proton transfer (APT) from proteins has generated particular interest, with applications in brain tumors (2–4), breast cancer (5–7), head and neck cancer (8), stroke (9), and Parkinson's disease (10). Also, relayed NOE (rNOE)-mediated CEST signals at −3.5 ppm (11–13) and the downfield-rNOE at 3.5 ppm resulting from the aromitc group (14) have been applied recently to the detection and evaluation of brain tumors.

While APT has attracted significant interest, the optimum acquisition method, metric, and quantitative approach are open questions, and there is effectively no gold standard. MTR_{asym} is the most well-established metric and is based on the difference between the signals acquired with irradiation at positive and negative offsets relative to the water resonance. Unfortunately, by combining signal contributions at negative and positive offsets, MTR_{asym} is unable to distinguish changes in APT (at +3.5 ppm) and rNOE (at −3.5 ppm). In addition, the macromolecular MT is asymmetric relative to the water resonance and thus creates a sloping negative baseline in the MTR_{asym} metric, further confounding APT quantification and making even visual identification of the APT contribution to the MTR_{asym} spectrum very difficult, especially at the lower field strengths relevant to human imaging studies. There have been several attempts to isolate the APT contribution to the Z-spectrum, including by fitting direct water saturation to a Lorentzian function (5–7,12,15,16), by fitting MT to multiple Lorentzian functions (17), and by the recently developed extrapolated semi-solid magnetization transfer reference method (EMR) (18,19) based on Henkelman's two-pool model (20,21). These fitting approaches implicitly assume underlying tissue models that may not adequately capture the drivers of signal changes, and hence may add confounding artificial contributions. Even if the modeling is accurate, these fitting approaches require acquisitions at a large number of frequency offsets far from the amide resonance, hence increasing scan time while acquiring data with no direct information on amide content or exchange rate. Ideally, we would like an imaging acquisition strategy and metric that, in human imaging studies, can give a direct and clear measure of amide contributions with minimal tissue assumptions and in a reasonable acquisition time.

Chemical exchange rotation transfer (CERT) (22–26) is an alternative acquisition strategy and set of imaging metrics that compares signals acquired at a single offset frequency, and hence is able to quantify APT and rNOE effects separately without mixing them (as in MTR_{asym}) and without tissue model assumptions (as in EMR and other fitting approaches). The approach is based on the assumption that there are both solute rotation and saturation contributions to the water signal, while the semi-solid MT pool only contributes to the water signal via macromolecular saturation. (Both rotation and saturation contribute to direct water effects.) By subtracting signals acquired using two different irradiation flip angles, yet the

same average irradiation power, contributions from MT effects and direct water saturation cancel, while contributions from solute rotation remain, hence isolating solute effects.

In this study, we will determine if the CERT approach (and the corresponding MTR_{double} metric) is able to isolate APT and rNOE signal contributions in the human brain at 3 T. We will compare these results to the conventional MTR_{asym} metric and the recently developed EMR methods, in particular, $sEMR^1$, which uses a two-pool model (water and symmetric MT) to fit the positive offset region (7~14 ppm) (18). ($sEMR^1$ is considered to be more specific compared to other EMR fitting approaches (18).) We also investigate the effect of a WASSR B_0 correction (27) on these metrics.

Method

Theory

To calculate the CERT metric MTR_{double}, label and reference scans are acquired using trains of repeated π and 2π pulses, respectively (22–26). As long as the power is the same in both of these irradiation pulse trains, the label and reference signals will have the same contributions from semi-solid MT and direct water saturation at any given offset. Therefore, the pulse train employed in CERT needs to maintain the root of the mean square irradiation field:

$$B_{avg\ power} = \sqrt{\frac{1}{PTR}\int_0^{PTR} B_1^2 dt} = \sqrt{\frac{p_2}{dc}}\frac{\pi\theta}{\gamma \cdot p_1 \cdot PTR}, \quad \text{(Eq. 1)}$$

where B_1 is the amplitude of the pulse, γ is the gyromagnetic ratio of proton, and the pulse time of repetition (PTR) is the sum of the pulse width and the interleave delay. Duty cycle (dc) is the ratio of the pulse width to PTR, θ is the flip angle of the saturation pulse and p_1 and p_2 are used to characterize the pulse shape. p_1 is defined as the ratio of the average amplitude to the maximum amplitude, and p_2 is defined as the ratio of the average of the square of the amplitude to the square of the maximum of the amplitude.

MTR_{double} is defined by:

$$MTR_{double} = \frac{S_{2\pi}(\Delta) - S_{\pi}(\Delta)}{S_0}\Big|_{B_{avg\ power}}. \quad \text{(Eq. 2)}$$

$S_{\pi}(\Delta)$ and $S_{2\pi}(\Delta)$ are the signals at the offset Δ, with $\theta = \pi$ and 2π, respectively. S_0 is the signal of the control scan, which is acquired at a large offset (on the order of 100 kHz). MTR_{double} takes the difference between signals acquired at the same offset and average power in order to remove MT and direct water saturation effects and to isolate contributions from solute rotation.

For comparison, we also calculate MTR_{asym} and $sEMR^1$, defined by:

$$MTR_{asym} = \frac{S(-\Delta) - S(\Delta)}{S_0} \quad \text{(Eq. 3)}$$

and

$$sEMR^1 = Z_{EMR} - \frac{S(\Delta)}{S_0}, \quad \text{(Eq. 4)}$$

, where $S(\Delta)$ is the signal at the offset Δ with a continuous wave saturation. Z_{EMR} is depicted by Henkelman's two-pool model (20,21) containing a water pool and a semi-solid MT pools, where the MT pool is assumed having a super-Lorentzian lineshape and symmetric to water resonance. The rest of the parameters using in the two-pool model were obtained by fitting the signals measured within an offset range between 7 and 14 ppm (18,19).

Subjects

Four male and two female healthy subjects (ages: 27 – 51 years, mean: 37 years) consented before imaging and the studies were approved by the Vanderbilt institutional review board (IRB).

MRI

All the images were acquired on a 3.0 T Achieva scanner (Philips Healthcare, Best, The Netherlands) with body coil for transmission and a 32-channel head coil for reception. The pulse train in CERT is composed of a series of Gaussian pulses (p_1 = 0.415 and p_2 = 0.294), and the total length of the pulse train is 2 s. The duty cycle is 30% or 50%, and the average power is varied between 0.5 μT, 0.7μT, and 0.9 μT. For instance, according to Eq. 1, in the case of a 30% duty cycle with a 0.5 μT average power, the pulse peak amplitude is 1.68 μT and pulse widths in label and reference scans are 16.81 ms and 33.62 ms, respectively. The parameters used for other conditions are listed in Table 1. Spoilers (5 ms and 20 mT/m with alternating positive and negative amplitudes) were applied after each saturation pulse to remove the residual transverse magnetization. The results from these CERT experiments were then compared against those from traditional CEST experiments using near continuous wave saturation: 4 square pulses of 200 ms pulse duration, 2 μT pulse amplitude and 95% duty cycle. Each sequence pulse was followed by spoilers. A B_0 map was obtained with WASSR (27) using a 100 ms, 0.2 μT Gaussian pulse. The CERT images were acquired at the following offsets in order (in ppm): −750, −6, −5.5, −5, −4.5, −4, −750, −3.75, −3.5, −3.25, −3, −2.5, −750, −2, −1.5, −1, −0.5, 0, 0.5, 1, 1.5, 2, −750, 2.5, 3, 3.25, 3.5, 3.75, −750, 4, 4.5, 5, 5.5, 6 and −750. CEST-based images were acquired at the following offsets in order (in ppm): −750, −14, −13, −12, −11, −10, −9, −750, −8, −7, −6, −5.5, −5, −4.5, −4, −750, −3.5, −3, −2.5, −2, −1.5, −1, −0.5, −750, 0, 0.5, 1, 1.5, 2, 2.5, 3, −750, 3.5, 4, 4.5, 5, 5.5, 6, 7, 8, −750, 9, 10, 11, 12, 13, 14 and −750. WASSR images were acquired at the offsets between −1 and 1 ppm with the interval of 0.1 ppm. The CERT/CEST images acquired at −750 ppm were the control scans. The CEST, CERT and WASSR images were acquired with

a spin-echo single-shot EPI readout (TE/TR = 35 ms/3000 ms) with the reversal gradient for fat suppression (28). The Field-of-view was 230 mm × 230 mm, thickness 5 mm, voxel size 2.5 × 2.5 mm, and reconstruction resolution 1.8 × 1.8 mm.

Data processing

CEST, CERT, and WASSR images were coregistered using the a rigid registration algrithm (29). CEST and CERT images were normalized voxel-by-voxel by a linear interpolation of the control scans, and the B_0 inhomogeneity of CEST and CERT images were corrected by WASSR (27), where the B_0 shift is determined by the irradiation offset that minimizes the water signal. For sEMR[1] method (18), we chose a offset range of 7 to 14 ppm to fit the Henkelman's two-pool mode. The images were smoothed with a Gaussian filter with a standard deviation of 0.6 pixel. All the images were processing with MATLAB 2015b (The Mathworks Inc., Natick, MA, USA).

Simulation

The tolerances to B_0 and B_1 inhomogeneity at 3T were simulated with a two-pool model (water and solute). The spin dynamics were described by six coupled Bloch equations (23) and solved by the ODE45 solver in MATLAB 2015b. The pulse sequence parameters were: 2 s saturation duration, a 30% duty cycle and 0.5, 0.7 and 0.9 μT average powers. The solute pool parameters were: T_1 = 1.5 s, T_2 = 0.015 s, exchange rate = 50 Hz, offset = 3.5 ppm, pool size ratio = 0.001, water pool T_1= 1.5 s, and water pool T_2 = 0.05 s.

Results

Representative CERT Z-spectra (averaging from 30 voxels in WM) with 0.5 μT average power and 30% duty cycle from one of the subjects are shown in Figure 1A. According to CERT theory (22–25), the reference scan ("2π" in figure legend) has contributions from solute, macromolecule, and water saturation. In contrast, the label scan ("π" in figure legend) has contribution from all of these saturation effects, and also has contributions from solute and water rotation. Figure 1B plots the normalized difference between the label and reference scans, isolating the effects of solute and water rotation. While the contributions from water rotation cause artifactual effects in the resulting MTR_{double} metric at small offsets, the effects from solute rotation create MTR_{double} peaks near 3.5 ppm (APT) and −3.5 ppm (rNOE). Note also that the MTR_{double} signal approaches a small offset ($\lesssim$ 1%) at large offsets where contributions from MT and direct water saturation are similar in the label and reference scans (see Figure S1).

We examined MTR_{double} with various average powers (0.5, 0.7, and 0.9 μT) and duty cycles (30% and 50%), and the corresponding pulse amplitudes and durations under these conditions are listed in Table 1. The MTR_{double} spectra shown in Figure 2 were averaged from WM of six subjects. In general, MTR_{double} using a 30% duty cycle is higher than it is using a 50% duty cycle, though this increase may be due to an apparent increase in the baseline contributions. CERT has a different dependence on duty cycle than does CEST, since only CERT isolates the spin rotation effect by taking the signal difference of scans with different pulse flip angles but the same average irradiation power. The resulting metric

is a complex function of irradiation time, power, and exchange rate (24). A lower duty cycle has a higher B_1 amplitude and results in magnetization rotation with less damping. It has been shown that MTR_{double} also depends on exchange rates and saturation powers (24). In our results, rNOE (exchange rate < 10 Hz) (14) signals, which include baseline contributions, reach a maximum when the average power is between 0.7 μT and 0.9 μT, while APT (exchange rate ≈ 30 Hz) (30) signals (including baseline) increase along with the average powers in the examined range (0.5 to 0.9 μT). We use the condition of a 0.5 μT average power and a 30% duty cycle in the following discussion since, with its small baseline, it yields distinct and clean signals for both APT and rNOE signals. While the goal of this work is a method that can give meaningful characterizations of amide and rNOE exchange effects using as few as one offset, a more complex approach using a three-Lorentzian model is evaluated in Supplementary Figure S2 and Table S1.

We also compared MTR_{double}, MTR_{asym}, and $sEMR^1$ in WM averaged over six subjects after WASSR B_0 correction (Figure 3A) and the effect of B_0 correction on these metrics in a typical subject (Figure 3B). MTR_{asym} and $sEMR^1$ were obtained using the same sequence and acquisition parameters as those in the original EMR paper (18). First note that the B_0 correction has a large effect on MTR_{asym} and $sEMR^1$, but a much smaller effect on MTR_{double}, effectively making application of a WASSR correction optional. After B_0-correction, MTR_{asym} is qualitatively similar to previously measured normal WM from subjects with a brain tumor (4,31,32). And, as in these previous studies, the baseline in MTR_{asym} provides confounding information, and there is no distinct peak at 3.5 ppm to indicate APT signal contributions. For $sEMR^1$, the peaks are not centered at the frequency of the exchanging sites (3.5 and −3.5 ppm). Also note the large negative values near −5 ppm, which were not seen in previous works (18) and may be due to varying degrees of MT asymmetry. In contrast to the other metrics, MTR_{double} has a flat and small baseline (especially near the amide resonance), making visible identification of the contributions from APT and, to a lesser degree, rNOE possible. Further, this small baseline and limited need for a WASSR B_0 correction, opens the possibility of getting meaningful APT or rNOE quantification with as few as three images, as required in Eq. 2.

The MTR_{double} and $sEMR^1$ images of APT (3.5ppm) and rNOE (−3.5ppm), and MTR_{asym} image (3.5 ppm) from one of the subjects are shown in Figure 4A, where the first and the second columns are with and without B_0 correction, respectively, and the third column is the difference between corrected and non-corrected images. For the corrected images, no obvious anatomical contrast is visible in the MTR_{double} images in normal tissue. MTR_{asym}, on the other hand, shows some white-matter/gray-matter contrast, which may reflect confounding MT contributions to the sloping baseline rather than contributions from APT or rNOE (4,31,33). The difference images, obtained by $Image_{corrected} - Image_{non-corrected}$, of MTR_{asym} and $sEMR^1$ (rNOE) are highly correlated to the B_0 map obtained with WASSR (Figure 4B). The histograms of “difference” images are shown in the last column in Figure 4(A). We fitted these histograms with a two-Gaussian model to roughly separate the regions with (shown in red) and without (shown in blue) a B_0 error corrected using the WASSR data. MTR_{asym} (3.5ppm), $sEMR^1$ (APT) and $sEMR^1$ (rNOE) are −1.4 ± 0.6%, −0.3 ± 0.1% and 0.9 ± 1.5%, respectively in the region with B_0 error, and in contrast MTR_{double} (APT) and MTR_{double} (rNOE) are 0.0 ± 0.3% and 0.0 ± 0.4%, respectively. The results show that

MTR_{double} is relatively insensitive to B_0 inhomogeneity, which confirms our previous simulations (24).

We estimated the effect of B_0- and B_1-imhomogeneities on MTR_{double} using a two-pool model simulation, and the results are plotted in Figure 5 A and B, respectively. The simulation results for B_0 errors are in rough agreement with our *in vivo* results. Figure 4B indicates that most tissues have 0 or 12.8 Hz errors in B_0, as indicated by the WASSR results. (Note that we used the minimum signal point in the WASSR experiment to determine the B_0 value. Hence, our frequency correction had a resolution equal to the irradiation offset spacing of 12.8 Hz.) The resulting difference in the MTR_{double} values for APT with and without WASSR correction (as plotted in Figures 4A) are a couple of percent of M_0, which roughly matches the 0.02 difference (indicated in Figure 5A) in the MTR_{double} simulated signal using 0.5 μT average irradiation power and a 12.8 Hz B_0 error. MTR_{double} when irradiating using 0.7 μT average power shows a qualitatively similar dependence on B_0 as in the 0.5 μT case and is similar to our previous simulation at 9.4T (24). However, when irradiating at 0.9 μT average power near 3.5 ppm offset, the contributions from direct water rotation become dominant and this effect changes the shape of the B_0 dependence. These direct water rotation effects at 3T also contribute to the baseline in Figure 2 and cause MTR_{double} to have a much greater dependence on B_1 (as seen in figures 5B) than is the case in previously published work at 9.4T (24).

Discussion

Several approaches have been proposed to remove background semi-solid MT based on the fitting of analytical models (17–19). Compared with the conventional metric, MTR_{asym}, which has a sloping baseline that confounds signal specificity, these metrics have a flatter baseline that facilitates greater metabolic specificity. Our MTR_{double} metric extends this further, having a relatively simple baseline that decays to zero at large offsets and has reasonable amplitudes (especially at low irradiation powers) at ±3.5 ppm (Figure 1B). The separation of APT and rNOE signal contributions from the baseline is especially clear at 30% duty cycle and a 0.5 μT average power (Figure 2A), where MT and direct water saturation effects are likely largely removed. However, the MTR_{double} theory indicates that direct water rotation may still contribute to the signal (24), and this confounding effect increases at higher average powers.

A key issue in developing clinically viable CEST imaging methods is the interplay between specificity and acquisition time. In order to avoid confounding baseline signal contributions, time-consuming calibration measurements (e.g. imaging B_0) and data intensive model fittings are typically required. For example, B_0 correction has become a standard procedure for CEST-based techniques to minimize the influence of field inhomogeneity. Our results show that B_0 correction is important when acquiring MTR_{asym} and $sEMR^1$ metrics, but produces only small changes in the MTR_{double} metric (Figures 3 and 4). Since mapping B_0 using the WASSR method requires low-power irradiation at roughly ten to twenty offsets around the water resonance, its inclusion significantly increases the experiment time, further hindering the feasibility of CEST in the clinics. Further, methods (such as $sEMR^1$) that rely on model fittings to remove confounding non-specific signal contributions require time-

consuming acquisitions at a wide range of offsets. In contrast, MTR_{double} involves no model fittings. In addition, unlike MTR_{asym}, MTR_{double} only compares signals at a single offset frequency. Hence, if WASSR B_0 is excluded, MTR_{double} only requires three scans (control, reference and labeling scans) to obtain an APT or rNOE signal. Thus, MTR_{double} has a much greater potential than other CEST metrics for very rapid, and therefore clinically viable, imaging. However, note that when acquiring MTR_{double} at only a single offset, no qualitative (or quantitative) assessment of the magnitude of the confounding baseline contributions is possible. Further, MTR_{double} at 3T has a significant dependence on B_1 (Fig. 5B), making any quantitative assessment suspect without a B_1 correction.

The APT and rNOE contrasts between grey and white matter are controversial. With the MTR_{double} metric, we did not find significant APT and rNOE contrast, and this result is consistent with our previous work in animals at 9.4T (25). In that work we ascribed the minimal gray/white contrast to the greater specificity of MTR_{double}, and we show that the much larger gray/white contrast reported using the CEST MTR_{asym} metric at the amide resonance is actually due to MT and NOE effects. However, even when limited to using CEST approaches, large variations in contrast have been reported. Jones et al. (12) found the maximum and minimum contrasts are rNOE (−3.3 ~ −3.7 ppm) and APT (3.3 to 3.7 ppm), respectively, among the offset ranges they investigated. Xu et al. (34) found APT has a hyperintensity in grey matter, but the rNOE contrast is negligible. Heo et al. (16) found APT is quite uniform but there is a rNOE contrast. They suspect the rNOE contrast is caused by the residual MT effect with their approach. Khlebnikov (35) et al. found no APT contrast but a rNOE contrast with hyperintensity in white matter. The approaches and metrics utilized among these literatures are quite different. In sum, the interplay between the pulse sequence and metric details and the underlying basis for white/gray contrast (or non-contrast) is still an active research area.

One of the challenges of applying CEST or CERT techniques in human studies is the limited chemical shift between water and exchanging solutes, which is 450 Hz for amides at 3T. This separation is much smaller than typical semi-solid MT linewidths, which is why many methods attempt to cancel these confounding effects. Further, while the amide-water separation is larger than the broadening from typical pulse widths, T_2, or B_1, it takes only a small contamination from direct water effects to overwhelm the relatively modest (~1%) contributions to the water signal from solute exchange. Further, as in conventional CEST studies, MTR_{double} measures of amide exchange may include contributions from downfield-rNOE at 3.5 ppm (14).

While CERT methods cancel direct water saturation by maintaining the same average power in the label and reference scans, there is no cancelation of direct water rotation, which may hence cause baseline contributions, and these confounding signal contributions are particularly problematic at lower field strengths, such as in human 3T studies. This effect increases when the average power is high, as shown in Figure 2, which motivates the use of a small (0.5 μT) average power. Further, while our recently developed CERT metrics ($MTR_{double, vdc}$ and $AREX_{double, vdc}$) maximize exchange sensitivity and avoid confounding T_1 contributions (26), the variations in their baseline signals are not yet determined. Hence, for this study we stuck with the more established MTR_{double} metric..

Conclusion

In this study, we apply CERT to human imaging at 3T and calculate the MTR_{double} metric. Using a 0.5 μT average power and a 30% duty cycle, we can obtain distinct and clear APT and rNOE peaks. This visually clear indication of APT and rNOE effects simplifies data interpretation compared to methods (such as MTR_{asym}) where sloping baselines make APT and MT contributions to the signal difficult to delineate or methods (such as $sEMR^{[1]}$) that require many acquisitions and corresponding model fittings. Further, with its relatively small confounding baseline signal (especially near the amide resonance), insensitivity to B_0 inhomogeneity, and absence of model fitting of tissue parameters, MTR_{double} can acquire meaningful APT or rNOE images in as little as three acquisitions: a control, a reference, and a label scan at a single frequency offset. However, sensitivity to B_1 at 3T may limit quantitative interpretations.

Supplementary Material

Refer to Web version on PubMed Central for supplementary material.

Acknowledgments

Grant Sponsor: T32EB001628, R01CA184693 and R01EB017767

We thank Kevin Wilson, MESc for assisting data processing.

References

1. Zhou J, Zijl PCMv. Chemical exchange saturation transfer imaging and spectroscopy. Prog Nucl Magn Reson Spectrosc. 2006; 48:109–136.
2. Zhao X, Wen Z, Huang F, Lu S, Wang X, Hu S, Zu D, Zhou J. Saturation power dependence of amide proton transfer image contrasts in human brain tumors and strokes at 3 T. Magn Reson Med. 2011; 66:1033–1041. [PubMed: 21394783]
3. Zhou J, Blakeley JO, Hua J, Kim M, Laterra J, Pomper MG, van Zijl PC. Practical data acquisition method for human brain tumor amide proton transfer (APT) imaging. Magn Reson Med. 2008; 60:842–849. [PubMed: 18816868]
4. Jones CK, Schlosser MJ, van Zijl PC, Pomper MG, Golay X, Zhou J. Amide proton transfer imaging of human brain tumors at 3T. Magn Reson Med. 2006; 56:585–592. [PubMed: 16892186]
5. Dula AN, Arlinghaus LR, Dortch RD, Dewey BE, Whisenant JG, Ayers GD, Yankeelov TE, Smith SA. Amide proton transfer imaging of the breast at 3 T: establishing reproducibility and possible feasibility assessing chemotherapy response. Magn Reson Med. 2013; 70:216–224. [PubMed: 22907893]
6. Klomp DWJ, Dula AN, Arlinghaus LR, Italiaander M, Dortch RD, Zu Z, Williams JM, Gochberg DF, Luijten PR, Gore JC, Yankeelov TE, Smith SA. Amide Proton Transfer Imaging of the Human Breast at 7 Tesla: Development and Reproducibility. NMR Biomed. 2013; 26:1271–1277. [PubMed: 23559550]
7. Dula AN, Dewey BE, Arlinghaus LR, Williams JM, Klomp D, Yankeelov TE, Smith S. Optimization of Chemical Exchange Saturation Transfer (CEST) Parameters at 7 Tesla for Validation of GAG- and APT-CEST Measurements of Fibroglandular Tissue of the Breast. Radiology. 2015; 275:255–261. [PubMed: 25353249]
8. Yuan J, Chen S, King AD, Zhou J, Bhatia KS, Zhang Q, Yeung DK, Wei J, Mok GS, Wang YX. Amide proton transfer-weighted imaging of the head and neck at 3 T: a feasibility study on healthy human subjects and patients with head and neck cancer. NMR Biomed. 2014; 27:1239–1247. [PubMed: 25137521]

9. Tee YK, Harston GW, Blockley N, Okell TW, Levman J, Sheerin F, Cellerini M, Jezzard P, Kennedy J, Payne SJ, Chappell MA. Comparing different analysis methods for quantifying the MRI amide proton transfer (APT) effect in hyperacute stroke patients. NMR Biomed. 2014; 27:1019–1029. [PubMed: 24913989]
10. Li C, Peng S, Wang R, Chen H, Su W, Zhao X, Zhou J, Chen M. Chemical exchange saturation transfer MR imaging of Parkinson's disease at 3 Tesla. Eur Radiol. 2014; 24:2631–2639. [PubMed: 25038850]
11. Xu J, Yadav NN, Bar-Shir A, Jones CK, Chan KW, Zhang J, Walczak P, McMahon MT, van Zijl PC. Variable delay multi-pulse train for fast chemical exchange saturation transfer and relayed-nuclear overhauser enhancement MRI. Magn Reson Med. 2014; 71:1798–1812. [PubMed: 23813483]
12. Jones CK, Huang A, Xu J, Edden RA, Schar M, Hua J, Oskolkov N, Zaca D, Zhou J, McMahon MT, Pillai JJ, van Zijl PC. Nuclear Overhauser enhancement (NOE) imaging in the human brain at 7T. Neuroimage. 2013; 77:114–124. [PubMed: 23567889]
13. Mehrabian H, Desmond KL, Soliman H, Sahgal A, Stanisz GJ. Differentiation between Radiation Necrosis and Tumor Progression Using Chemical Exchange Saturation Transfer. Clin Cancer Res. 2017; 23:3667–3775. [PubMed: 28096269]
14. Zaiss M, Windschuh J, Goerke S, Paech D, Meissner J-E, Burth S, Kickingereder P, Wick W, Bendszus M, Schlemmer H-P, Ladd ME, Bachert P, Radbruch A. Downfield-NOE-suppressed amide-CEST-MRI at 7 Tesla provides a unique contrast in human glioblastoma. Magn Reson Med. 2017; 77:196–208. [PubMed: 26845067]
15. Jones CK, Polders D, Hua J, Zhu H, Hoogduin HJ, Zhou J, Luijten P, van Zijl PC. In vivo three-dimensional whole-brain pulsed steady-state chemical exchange saturation transfer at 7 T. Magn Reson Med. 2012; 67:1579–1589. [PubMed: 22083645]
16. Heo HY, Jones CK, Hua J, Yadav N, Agarwal S, Zhou J, van Zijl PC, Pillai JJ. Whole-brain amide proton transfer (APT) and nuclear overhauser enhancement (NOE) imaging in glioma patients using low-power steady-state pulsed chemical exchange saturation transfer (CEST) imaging at 7T. J Magn Reson Imaging. 2015; 44:41–50. [PubMed: 26663561]
17. Windschuh J, Zaiss M, Meissner JE, Paech D, Radbruch A, Ladd ME, Bachert P. Correction of B1-inhomogeneities for relaxation-compensated CEST imaging at 7 T. NMR Biomed. 2015; 28:529–537. [PubMed: 25788155]
18. Heo HY, Zhang Y, Jiang S, Lee DH, Zhou J. Quantitative assessment of amide proton transfer (APT) and nuclear overhauser enhancement (NOE) imaging with extrapolated semisolid magnetization transfer reference (EMR) signals: II. Comparison of three EMR models and application to human brain glioma at 3 Tesla. Magn Reson Med. 2016; 75:1630–1639. [PubMed: 26033553]
19. Lee DH, Heo HY, Zhang K, Zhang Y, Jiang S, Zhao X, Zhou J. Quantitative assessment of the effects of water proton concentration and water T changes on amide proton transfer (APT) and nuclear overhauser enhancement (NOE) MRI: The origin of the APT imaging signal in brain tumor. Magn Reson Med. 2016; 77:855–863. [PubMed: 26841096]
20. Morrison C, Mark Henkelman R. A model for magnetization transfer in tissues. Magn Reson Med. 1995; 33:475–482. [PubMed: 7776877]
21. Morrison C, Stanisz G, Henkelman RM. Modeling Magnetization Transfer for Biological-like Systems Using a Semi-solid Pool with a Super-Lorentzian Lineshape and Dipolar Reservoir. J Magn Reson. 1995; 108:103–113.
22. Zu Z, Li K, Janve VA, Does MD, Gochberg DF. Optimizing pulsed-chemical exchange saturation transfer imaging sequences. Magn Reson Med. 2011; 66:1100–1108. [PubMed: 21432903]
23. Zu Z, Janve VA, Li K, Does MD, Gore JC, Gochberg DF. Multi-angle ratiometric approach to measure chemical exchange in amide proton transfer imaging. Magn Reson Med. 2012; 68:711–719. [PubMed: 22161770]
24. Zu Z, Janve VA, Xu J, Does MD, Gore JC, Gochberg DF. A new method for detecting exchanging amide protons using chemical exchange rotation transfer. Magn Reson Med. 2013; 69:637–647. [PubMed: 22505325]

25. Zu Z, Xu J, Li H, Chekmenev EY, Quarles CC, Does MD, Gore JC, Gochberg DF. Imaging amide proton transfer and nuclear overhauser enhancement using chemical exchange rotation transfer (CERT). Magn Reson Med. 2014; 72:471–476. [PubMed: 24302497]
26. Zu Z, Li H, Xu J, Zhang X-Y, Zaiss M, Li K, Does MD, Gore JC, Gochberg DF. Measurement of APT using a combined CERT-AREX approach with varying duty cycles. Magnetic resonance imaging. 2017; 42:22–31. [PubMed: 28526431]
27. Kim M, Gillen J, Landman BA, Zhou J, van Zijl PC. Water saturation shift referencing (WASSR) for chemical exchange saturation transfer (CEST) experiments. Magn Reson Med. 2009; 61:1441–1450. [PubMed: 19358232]
28. Gomori J, Holland G, Grossman R, Gefter W, Lenkinski R. Fat suppression by section-select gradient reversal on spin-echo MR imaging. Work in progress. Radiology. 1988; 168:493–495. [PubMed: 3393670]
29. Viola P, Wells WM III. Alignment by Maximization of Mutual Information. Int J Comput Vis. 1997; 24:137–154.
30. Zhou J, Payen J-F, Wilson DA, Traystman RJ, van Zijl PC. Using the amide proton signals of intracellular proteins and peptides to detect pH effects in MRI. Nature medicine. 2003; 9:1085–1090.
31. Zhou J, Lal B, Wilson DA, Laterra J, van Zijl PC. Amide proton transfer (APT) contrast for imaging of brain tumors. Magn Reson Med. 2003; 50:1120–1126. [PubMed: 14648559]
32. Zhu H, Jones CK, van Zijl PC, Barker PB, Zhou J. Fast 3D chemical exchange saturation transfer (CEST) imaging of the human brain. Magn Reson Med. 2010; 64:638–644. [PubMed: 20632402]
33. Hua J, Jones CK, Blakeley J, Smith SA, van Zijl PC, Zhou J. Quantitative description of the asymmetry in magnetization transfer effects around the water resonance in the human brain. Magn Reson Med. 2007; 58:786–793. [PubMed: 17899597]
34. Xu X, Yadav NN, Zeng H, Jones CK, Zhou J, van Zijl PCM, Xu J. Magnetization transfer contrast–suppressed imaging of amide proton transfer and relayed nuclear overhauser enhancement chemical exchange saturation transfer effects in the human brain at 7T. Magn Reson Med. 2016; 75:88–96. [PubMed: 26445350]
35. Khlebnikov V, Siero JCW, Wijnen J, Visser F, Luijten PR, Klomp DWJ, Hoogduin H. Is there any difference in Amide and NOE CEST effects between white and gray matter at 7T? Journal of Magnetic Resonance. 2016; 272:82–86. [PubMed: 27662404]

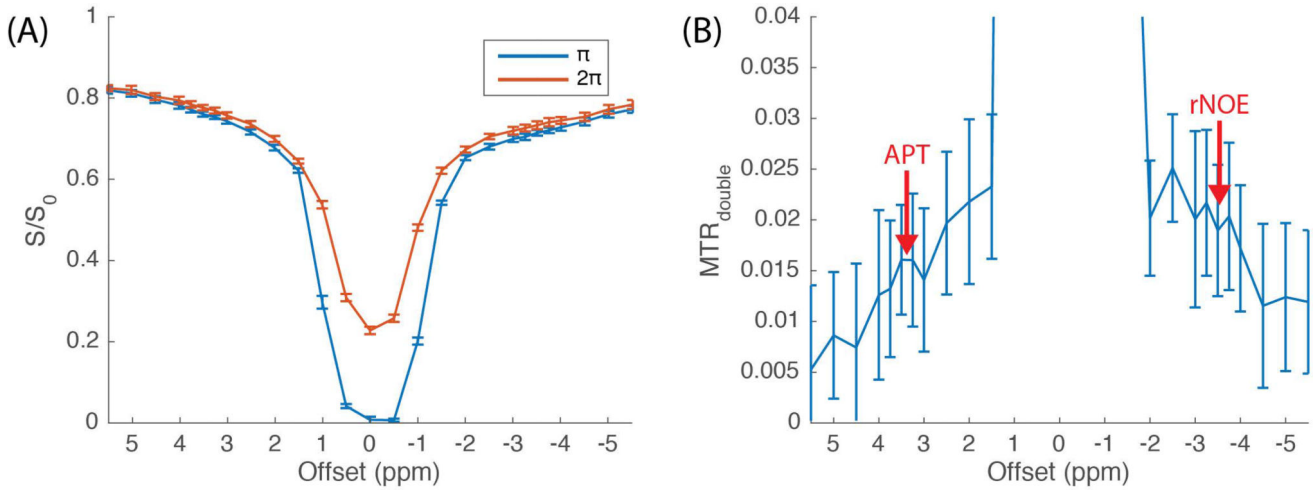

Figure 1.

Z-spectra of CERT (A) and MTR_{double} (B) were obtained with an average power of 0.5 μT and a duty cycle of 30% under the constraint in Eq. 1, and the signals were averaged from 30 voxels in WM from one of the subjects. APT and rNOE signal contributions are clear, on top of a small sloping baseline.

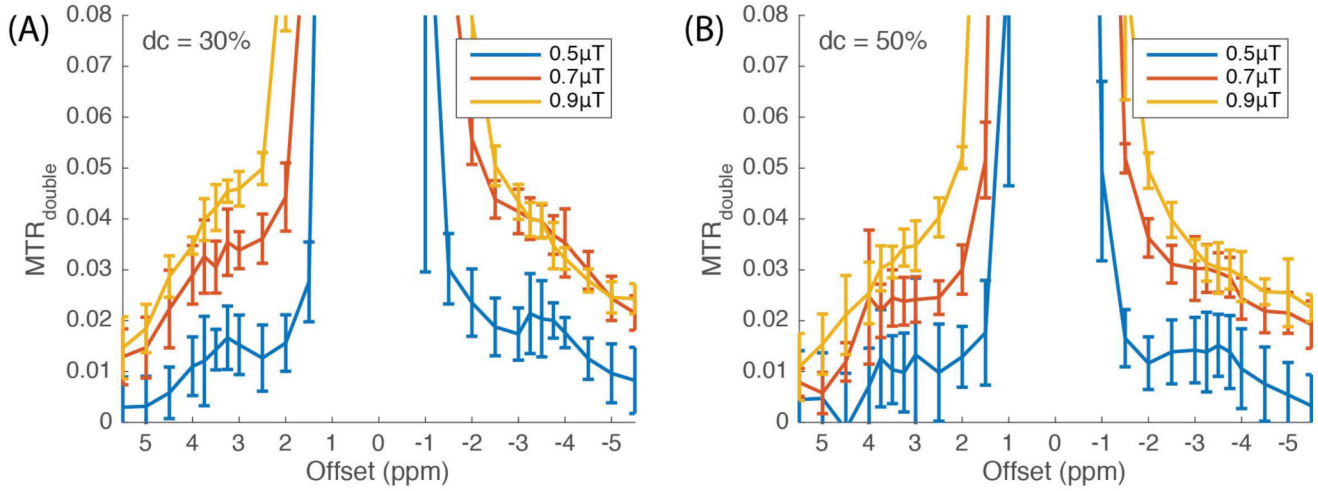

Figure 2.

A range of average irradiation powers were employed with a duty cycle of 30% (A) and 50% (B). The signals were averaged from 30 voxels in WM from six healthy subjects, respectively.

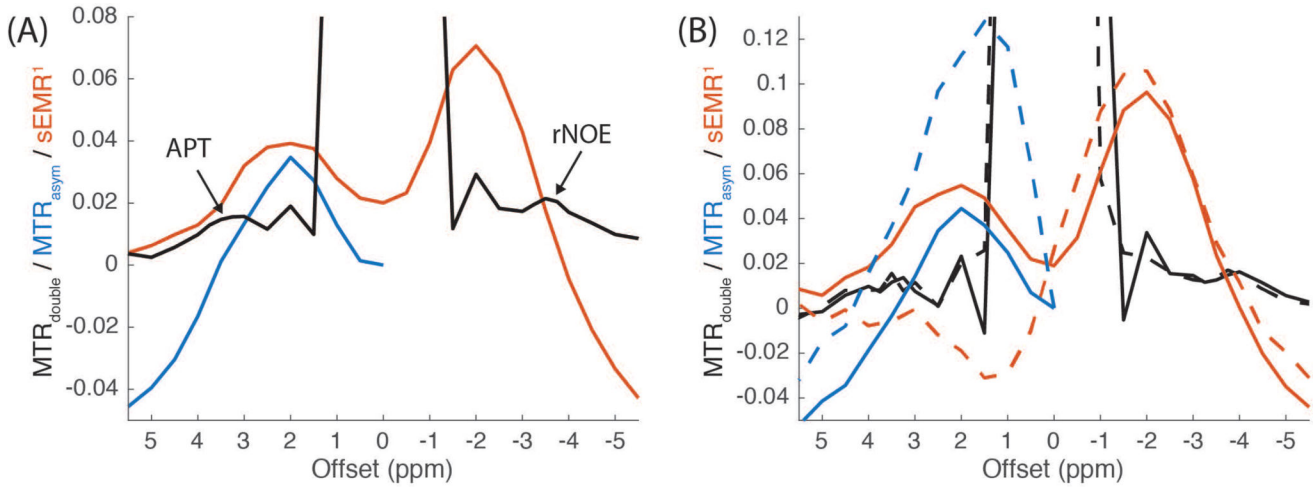

Figure 3.

The comparisons of MTR_{double} (black), MTR_{asym} (blue) and $sEMR^1$ (red) (A) and their changes corresponding to B_0 correction (B). The results with and without WASSR B_0 correction are shown in solid and dashed lines, respectively. The signals in (A) were averaged from WM in six healthy subjects, and the signals in (B) were averaged from WM of a single subject. MTR_{double} was obtained with a 0.5 μT average power and a 30% duty cycle. The results show that MTR_{double} has (1) a much flatter and smaller baseline, (2) much more distinct and visible peaks at the exchange sites (see arrows at 3.5 and −3.5 ppm), and (3) less sensitivity to B_0 inhomogeneity than do MTR_{asym} and $sEMR^1$.

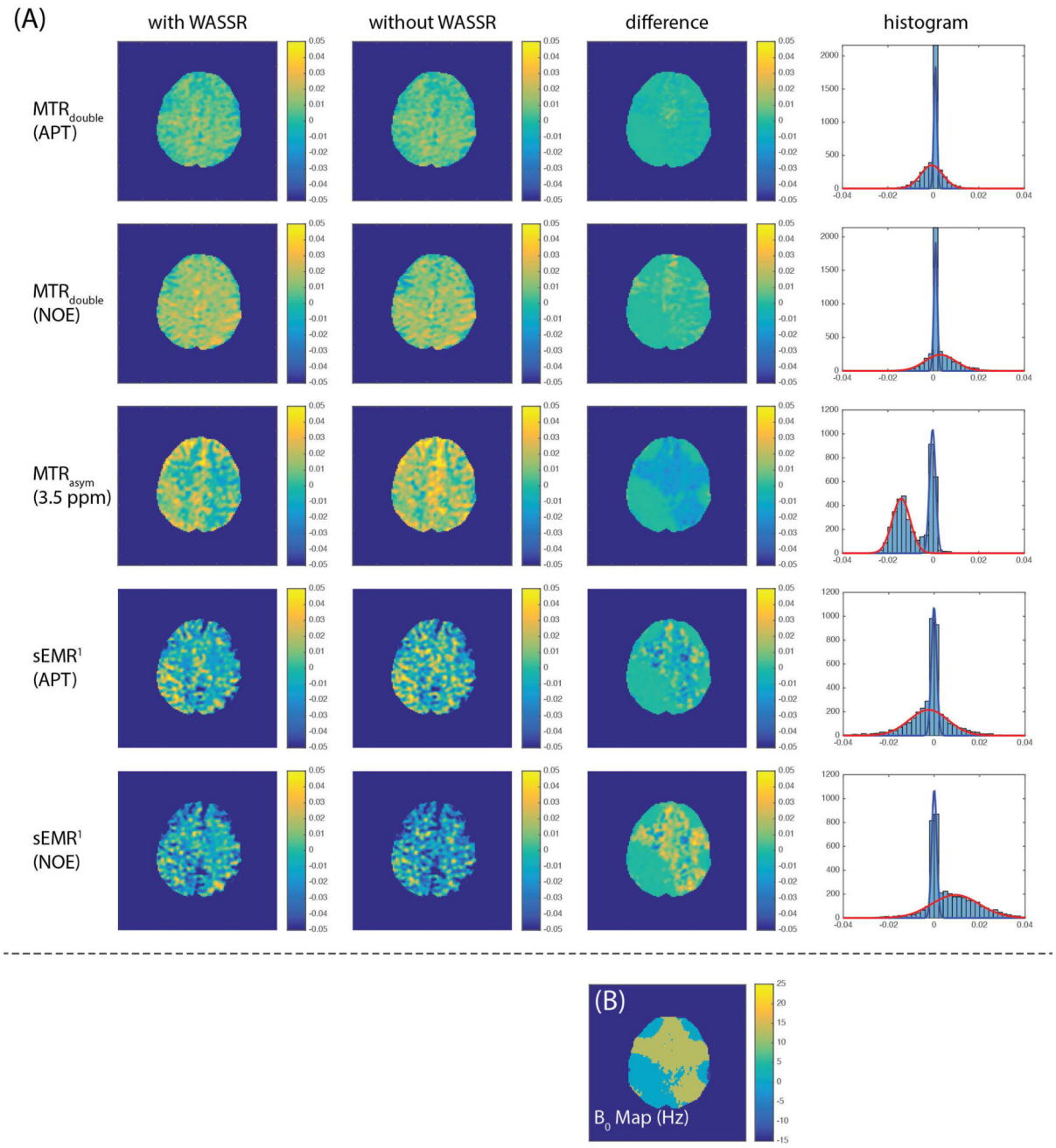

Figure 4.

CEST/CERT images (A) and B_0 map (B) from one of the subject. (A) The images in the first and second columns are with and without WASSR B_0 correction, respectively. The images in the third column are the differences between the first two columns. The histograms of "difference" images are shown in the last column. MTR_{double} was obtained with a 0.5 μT average power and a 30% duty cycle. The difference images are highly correlated to B_0 map (B), as expected. Note the very small magnitude of the MTR_{double} "difference" images, indicating a small dependency on B_0. Also note that the larger gray-matter/white-matter contrast in the MTR_{asym} image (compared to the MTR_{double} images) likely reflects

contributions from non-specific and confounding contributions from the sloping and non-zero baseline.

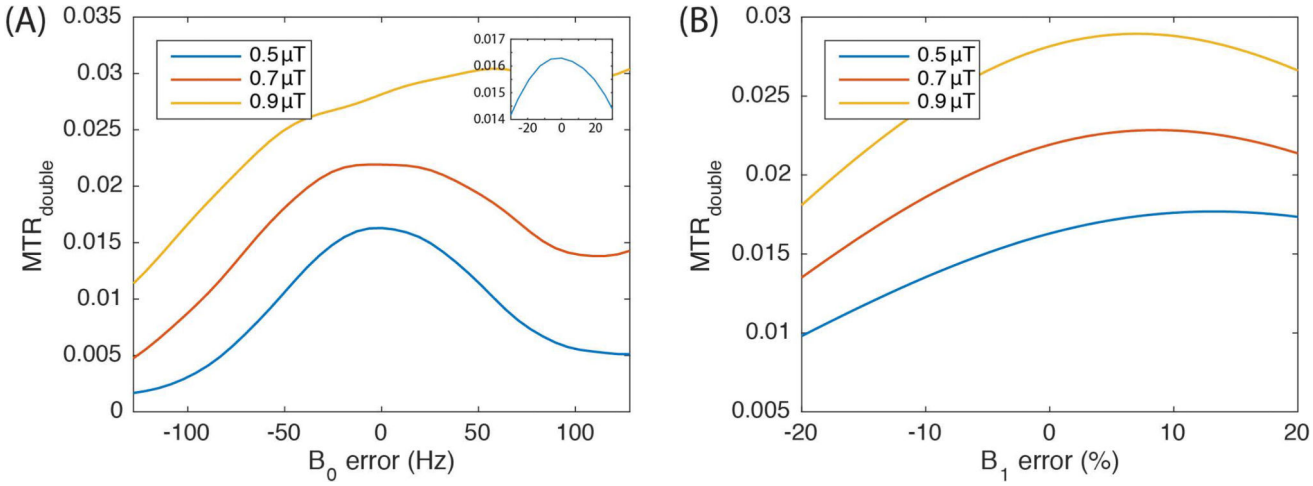

Figure 5.

Simulations of MTR_{double} at 3.5 ppm with B_0 (A) and B_1 (B) errors. Both simulations were obtained with a two-pool model (water and solute at 3.5 ppm). The inset in (A) expands the y-axis scale for B_0 variations between −20 and 20 Hz.

Table 1

The list of the pulse train of repetitions (PTR), pulse widths (pw), and the pulse peak amplitude (B_1) of the corresponding duty cycle (dc) and average power ($B_{avg\ power}$) for the label scans in CERT. For the corresponding reference scans, the lengths of PTR and pw are doubled, and B_1 is the same.

dc	$B_{avg\ power}$ (μT)	PTR (ms)	pw (ms)	B_1 (μT)
30%	0.5	56.03	16.81	1.68
	0.7	40.03	12.01	2.35
	0.9	31.13	9.340	3.02
50%	0.5	43.40	21.70	1.30
	0.7	31.00	15.50	1.82
	0.9	24.12	12.06	2.34